

# A vortex dipole in a trapped two-dimensional Bose-Einstein condensate

Weibin Li, Masudul Haque, and Stavros Komineas

Max Planck Institute for Physics of Complex Systems, Nöthnitzer Strasse 38, Dresden, Germany

(Dated: September 2, 2021)

We study the conservative dynamics and stationary configurations of a vortex-antivortex pair in a harmonically trapped two-dimensional Bose-Einstein condensate. We establish the conceptual framework for understanding the stationary states and the topological defect trajectories, through considerations of different mechanisms of vortex motion and the bifurcation of soliton-like stationary solutions. Our insights are based on Lagrangian-based variational calculations, numerical solutions of both the time-dependent and time-independent Gross-Pitaevskii equations, and exact solutions for the non-interacting case.

## I. INTRODUCTION

Vortex-antivortex pairs or *vortex dipoles* are ubiquitous in two-dimensional (2D) Bose condensates. They are the most natural excitations when a 2D fluid flows past a barrier or through a disordered medium. Such creation of vortices and antivortices has been seen explicitly in recent experiments with trapped atomic condensates [1]. In 2D, vortex dipoles can be thermally created. This is important for the thermodynamics of a 2D superfluid, *e.g.*, for the Kosterlitz-Thouless phase transition recently studied experimentally [2]. Given their pervasiveness and the current experimental interest with harmonically trapped condensates, a thorough study of vortex dipoles in trapped condensates is clearly important.

In this Article, we use a combination of methods to analyze vortex-antivortex states and dynamics in a circularly trapped 2D condensate, as described by the time-dependent Gross-Pitaevskii equation (GPE). First, we use a variational approach to the GPE that can be solved almost analytically, providing qualitative insight. These insights are explored and complemented by explicit numerical evolutions of the time-dependent GPE, exact solutions for the non-interacting case, and a numerical procedure for accessing stationary solutions of the time-independent GPE. Our results indicate that the dynamics of a vortex-antivortex pair in a trap is unexpectedly rich. In this Article we focus on a subset of possible dynamics, namely, the pair trajectory for cases where the pair is initially placed symmetrically on opposite sides of the trap center.

The physics behind our characteristic pair trajectories involves two effects. First, a vortex dipole in a large fluid body is a *propagating* object, *i.e.*, the vortex and antivortex propel each other in a direction perpendicular to the line joining them. This has been studied in condensates [3, 4] and is also common experience for ordinary fluids. In a trapped non-rotating condensate, there is an additional effect. An off-center vortex is known to precess around the center of the trap [5, 6]; we can regard this as inhomogeneity-driven motion. For a vortex dipole in a trap, each of the pair is driven by the inhomogeneity, in a direction opposite to the mutually-

driven motion. One of the two types of motion, mutually driven or inhomogeneity-driven, can dominate, depending on the vortex-antivortex distance. This leads to the remarkable fact that a vortex dipole with the same sense (same dipole direction) can be propagating in one of two opposite directions, depending on the dipole separation. A similar situation holds for vortex rings in 3D trapped condensates [7, 8]. Another result of the competition described above is that the two effects can in some cases exactly balance each other, leading to *stationary configurations* of vortex pairs. In this Article, we will examine in detail effects of this competition, for a vortex dipole in a circularly trapped condensate.

The conservative dynamics presented here should be accessible experimentally, *e.g.*, by creating a vortex-antivortex pair by phase imprinting, analogous to the first creation of a vortex in a laser-cooled condensate [9]. In contrast, the recent experiments [1, 2] deal with *dissipative* physics involving creation and destruction of vortex dipoles. While we have omitted dissipative considerations in this study, we will see that the conservative dynamics is extremely rich by itself.

Theoretically, vortex dipoles in trapped condensates have appeared as a peripheral topic in numerical studies of 3D vortex rings [7, 8, 10, 11, 12], which may be regarded as 3D analogs of 2D vortex dipoles. Refs. [13, 14] have considered stationary vortex dipole states, which we will further examine and interpret, Ref. [15] has studied energetics, while Ref. [16] presented some density dynamics. Very recently, Ref. [17] has studied some vortex dipole dynamics in the weak-interaction region.

Sec. II presents results from our variational calculation. Although the variational results cannot be expected to be quantitatively accurate, the calculation provides physical intuition. In particular, the most prominent feature of the vortex dipole trajectories, involving each singularity revolving around a stationary point, already emerges from this calculation. In Sec. III we present relevant exact results for the non-interacting case, focusing again on defect trajectories. Sec. IV presents numerical solutions of the time-independent GPE. This provides valuable insight into the differences observed in the dynamics for small interactions and large interactions. In Sec. V we present direct numerical simulations of the time-dependent GPE. The earlier calculations (Secs. II,

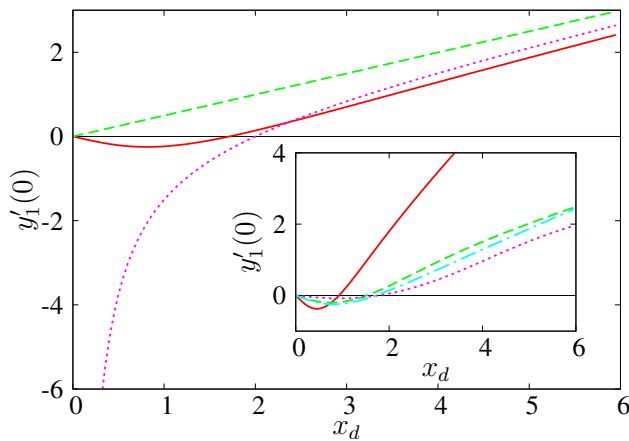


FIG. 1: (Color online.) Initial pair velocities versus dipole separation. Thick-solid: Gaussian ansatz,  $g = 0.1$ . Dashed: a single vortex, same ansatz, same  $g = 0.1$ . Dotted line: non-interacting condensate,  $\frac{1}{2}x_d - 2/x_d$ . Inset: Initial velocities versus  $x_d$ , Solid, dashed and dotted-dashed lines are from Thomas-Fermi ansatz, with  $g = 1, 10$ , and  $100$ . Dotted line is from gaussian ansatz,  $g = 1$ . All quantities are plotted in trap units.

III, IV) allow us to interpret the results of the time-dependent simulations; Secs. VI and VII present the interpretations and point out open questions.

*Gross-Pitaevskii Equation.* We study a low-temperature Bose-Einstein condensate in a harmonic trap. From the outset we start with a two-dimensional system confined to the  $xy$  plane, assuming that the dynamics in the  $z$  direction is frozen out by tight confinement which we do not treat explicitly. We will consider circular traps, and measure lengths in units of trap oscillator length, and measure lengths in units of trap oscillator length and time in units of inverse trapping frequency. The condensate dynamics is given by the time-dependent Gross-Pitaevskii equation [18, 19]:

$$i \frac{\partial \psi(t)}{\partial t} = -\frac{1}{2} \nabla^2 \psi + V_{\text{tr}}(\mathbf{r})\psi + g|\psi|^2\psi. \quad (1)$$

The trap potential is  $V_{\text{tr}} = \frac{1}{2}(x^2 + y^2)$ . The effective 2D interaction strength  $g$  characterizes the two-body interaction, but also depends proportionally on the total particle number  $N$  and inversely on the oscillator length.

## II. INSIGHTS FROM VARIATIONAL CALCULATION

In this Section we will draw physical insights from a time-dependent variational calculation. This is not expected to give quantitative predictions, but will provide valuable intuition about the stationary solutions and characteristic trajectories of the vortex dipole. We use the following class of simple variational wavefunctions:

$$\psi = A(t) [z - z_1(t)] [z^* - z_2^*(t)] f_c(|z|^2), \quad (2)$$

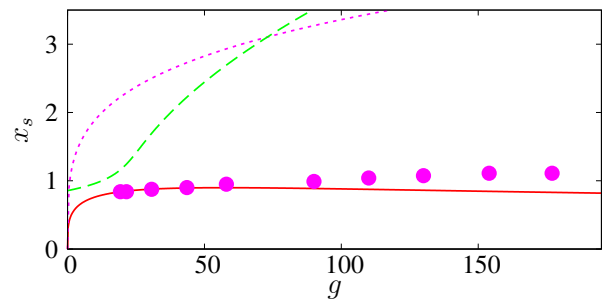


FIG. 2: (Color online.) Half-distance between pair for stationary vortex dipole configuration,  $x_s$ , as function of  $g$ . Solid line: from Thomas-Fermi ansatz; dashed line from Gaussian ansatz; filled circles from time-independent GPE. The dotted line shows the Thomas-Fermi boundary of condensate. Lengths are plotted in trap units.

where  $z = x + iy$  is the complex 2D position coordinate,  $z_1$  and  $z_2$  are vortex and antivortex positions, and  $A(t)$  is a normalization constant. Both Gaussian and Thomas-Fermi forms are used for the condensate shape function  $f_c$ . Details of the formulation are in the Appendix.

Our form (2) is amenable to exact treatment. Its disadvantage is that the vortices are ‘too big’, being determined by the trap size rather than the healing length  $\xi$ , which is reasonable only for small interactions. We note however that in two dimensions  $\xi \sim g^{-1/4}$  decreases rather slowly with the interaction parameter, so that vortices remain big even for relatively large values of  $g$ . For the physics of stationary states, our wavefunctions therefore give good answers up to large  $g$  (up to  $g \sim 90$ ). The situation with dynamics is more complicated.

### A. Stationary solution

We restrict ourselves to initial positions of the vortex and antivortex which are symmetric around the trap center; without loss of generality we place both on the  $x$ -axis,  $y_1(0) = y_2(0) = 0$ . If we start with  $x_2(0) = -x_1(0) < 0$ , mutually-driven (inhomogeneity-driven) motion would tend to drive both defects in the negative (positive)  $y$  direction. Mutually-driven (inhomogeneity-driven) motion wins when the vortex and antivortex are close to (far from) each other. Fig. 1 displays this competition by plotting the initial velocity,  $y'_1(0) = y'_2(0)$ , against the initial dipole separation,  $x_d = 2x_1(0)$ . The initial velocity is negative (positive) for smaller (larger)  $x_d$ .

We also note that the vortex dipole initial velocity approaches that of a single vortex, placed at  $x_1(0) = x_d/2$ , when the distance is large enough, demonstrating that the motion of the two defects are indeed determined primarily by the trap shape when they are far enough apart.

At some intermediate distance, the two effects balance each other,  $y'_{1,2}(0) = 0$ . This nontrivial *stationary configuration* is a central theme of this work. We denote as  $x_s$  the stationary value of  $x_1(0) = x_d/2$ . We explain later

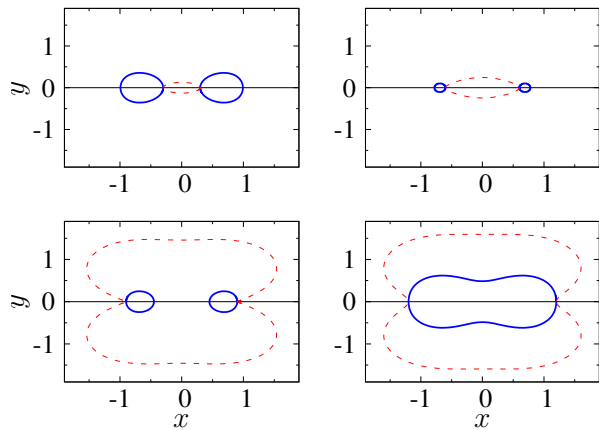


FIG. 3: (Color online.) Vortex and antivortex trajectories, calculated using the variational formalism with wavefunction (A.3). The four pictures show trajectories resulting from initial positions  $x_1(0) = 0.3, 0.6, 0.9, 1.2$ . Full and dashed lines show  $g = 6$  and  $g = 40$  respectively. Lengths are plotted in trap units.

that above a critical interaction  $g = g_c \approx 18.0$ , a vortex dipole configuration is a true stationary solution of the full Gross-Pitaevskii solution such that not only the singularity positions but also the density is stationary.

Fig. 2 shows the stationary point positions  $x_s$  as functions of the interaction strength  $g$ , calculated using the trial wavefunctions (A.2) and (A.3). Also shown are numerically exact values of  $x_s$ , calculated directly from the GPE (Sec. IV) for  $g > g_c \approx 18.0$ . The comparison shows that the gaussian ansatz is not useful in the relevant region  $g > g_c$ . The Thomas-Fermi ansatz (A.3) gives good results for the static solutions until  $g \sim 90$ . We will therefore restrict ourselves to this wavefunction in Sec. II B.

For very large  $g$ , the ansatz (A.3) yields decreasing behavior for the  $x_s(g)$  function, presumably due to the ‘large-vortex’ nature of our wavefunction.

### B. Trajectories

The full curves of Fig. 3 are vortex pair trajectories, calculated using the Thomas-Fermi wavefunction (A.3) for  $g = 6$ . When placed close together ( $x_1(0) < x_s$ ), the pair starts by moving in the negative  $y$  direction, due to mutually-driven dipole motion. As they move away from the  $x$ -axis, inhomogeneity-driven motion becomes more and more important, and eventually they turn away from each other and move in the positive  $y$  direction, crossing the  $x$ -axis at some  $x_1 > x_s$ . As they move in the  $+y$  direction, the distance between them decrease, and this causes the direction to reverse again. The reversals of motion might be regarded as ‘reflections’ of the propagating vortex dipole, at each ‘end’ of the trap.

The variational calculation gives periodic orbits for vortex and antivortex (first three panels of Fig. 3; left panel of Fig. 4). When the starting positions  $x_1(0)$  are

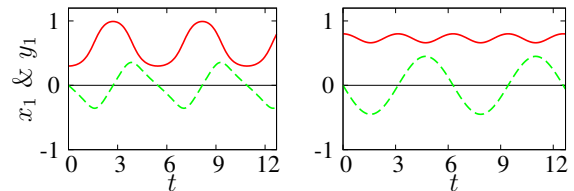


FIG. 4: (Color online.) Vortex position  $(x_1, y_1)$  as function of time. Left panel: variational calculation with Thomas-Fermi ansatz ( $g = 6$ ). Right panel: non-interacting bosons solved in terms of harmonic oscillator wavefunctions. All quantities are plotted in trap units.

moderately larger than  $x_s$ , a similar closed orbit pair results, starting from the outer edges of the closed trajectories. The closed orbits are smaller if the initial distance from the stationary point,  $|x_1(0) - x_s|$ , is smaller. The dashed lines and the last panel in Fig. 3 show unphysical features in trajectories with large  $g$  or large  $x_1(0)$ , which are artifacts of our simple variational setup.

We will show in Sec. V that the full Gross-Pitaevskii solution supports very similar trajectories for large  $g$ . Our simple variational approach has thus already uncovered a very characteristic motion of vortex dipoles in 2D trapped condensates, namely, trajectories in which the two defects each revolve around a stationary point.

### III. NON-INTERACTING BOSONS

The case  $g = 0$ , *i.e.*, non-interacting bosons in a harmonic trap, is exactly solvable. One can build any desired initial state as a linear combination of appropriate harmonic oscillator eigenstates. The evolution of each eigenstate is known — an eigenstate with energy  $E$  evolves as  $\phi(t) = \phi(0)e^{-iEt}$ . Therefore the evolution of any state can be found once it is expressed in this basis.

A state will be *stationary* only if it is built out of eigenstates with the same energy  $E$ . Considering the wavefunctions of a 2D harmonic oscillator (*e.g.*, Ref. [20]), it is easy to convince oneself that an off-center vortex-antivortex pair cannot be formed out of the eigenstates corresponding to a single energy. Thus a stationary vortex dipole configuration does not exist for  $g = 0$ .

However, one can form a quasi-stationary state in which the defect positions are stationary, although the condensate density undergoes complicated periodic motions. This is formed by combining eigenstates from the three lowest eigenvalues, so that there are off-center vortex and antivortex at  $(\pm x_1(0), 0)$ . It is straightforward to show  $y_1'(0) = x_1(0) - 1/x_1(0)$ , also plotted in Fig. 1. The quasi-stationary configuration is therefore  $x_s = 1$ .

The defect trajectories for  $g = 0$ , found from the above linear combination, involve sharp direction reversals along the same path. This suggests that the vortex picture is not very suitable here. In fact, the density profiles do not show well-defined vortex and antivortex, but

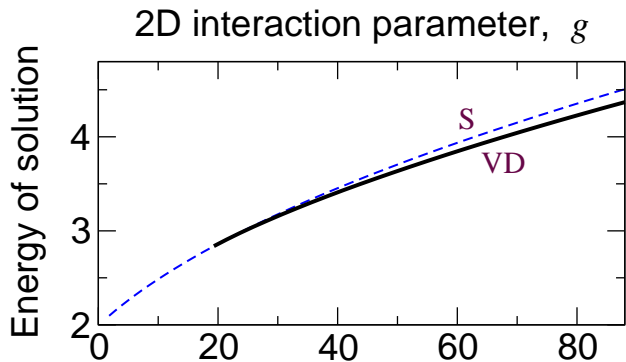


FIG. 5: (Color online.) The stationary soliton solution bifurcates at  $g \approx 18$ , producing a stationary vortex dipole solution. Dashed (full) line shows energy of a stationary soliton (stationary vortex dipole).

a ‘soliton’-like band of low density, even when the system contains a dipole-like pair of singularities at  $(\pm x_1(0), 0)$ .

The right panel of Fig. 4 shows the defect trajectories for the 2D non-interacting trapped condensate, via the functions  $x_1(t)$  and  $y_1(t)$ . The  $x_1(t)$  curve has half the period of  $y_1(t)$ , indicating that the defects move back and forth along the same line instead of around a closed orbit.

#### IV. STATIC SOLUTIONS: SOLITONS & VORTEX DIPOLES

The absence of a vortex-antivortex stationary solution for  $g = 0$ , and some of the dynamics to be presented in Sec. V, can be put into context by considering a bifurcation phenomenon [13].

At small  $g$ , we do have a stationary solution: a dark soliton-like object instead of a vortex dipole. This is easy to see for  $g = 0$ : the first-excited  $(n_x, n_y) = (0, 1)$  eigenstate,  $\psi_{01} \propto y e^{-(x^2+y^2)/2}$ , can be regarded as a dark soliton analog. The term ‘soliton’ comes from the analogy to the case where the confinement in the  $y$  direction is much weaker, *i.e.*, a ‘quasi-1D’ condensate. Although the word evokes a picture of a propagating object, in a trapped condensate a soliton can be stationary.

As  $g$  is increased, the soliton-like configuration remains a stable stationary object until  $g = g_c$ , at which point it bifurcates into two solutions, of which the unstable one is still soliton-like and the stable one is the vortex dipole configuration. Using a many-variable Newton-Raphson method to find solutions of the time-independent GPE, we have found that the point above which the stationary vortex dipole exists is  $g_c \approx 18$ . This is consistent with Ref. [13], but provides better precision. The energies of the soliton solution and the vortex dipole solution are shown in Fig. 5 as a function of  $g$ , and density profiles for stable stationary solutions are in Fig. 6.

The same bifurcation happens in elongated traps, where the word ‘soliton’ is more appropriate. In a 3D

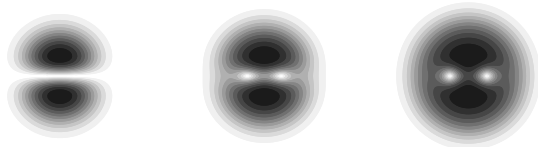


FIG. 6: Density profiles of stationary states: (1) soliton at  $g = 11$ ; (2) vortex dipole at  $g = 25$ ; (3) vortex dipole at  $g = 60$ .

trap one gets via bifurcation a stationary *vortex ring* instead of a vortex dipole [7].

The filled circles in Fig. 2 indicate stationary vortex dipole positions for  $g > g_c$ . Note that the value of  $x_s$  is near the trap oscillator length ( $x_s \approx 1$ ) over a wide range of  $g$ . This is well below the Thomas-Fermi size of the system (dotted line in Fig. 2), which increases as  $R_{\text{TF}} \sim g^{1/4}$  with the interaction.

#### V. NUMERICAL EVOLUTION OF GROSS-PITAEVSKII EQUATION

We now present results from explicit numerical evolutions of the 2D time-dependent Gross-Pitaevskii equation. In these simulations, a vortex dipole was first created at  $x = \pm x_d/2$  by propagating in imaginary time, at each step normalizing and also imposing the phase structure of  $(z - z_1)(z^* - z_2^*)$ . After reaching a stable dipole configuration, propagation in real time was followed. Time propagation was performed using the 4th-order Runge-Kutta algorithm, with the kinetic energy term calculated in momentum space.

Since we have no dissipation, the energy should remain constant. Breakdown of the numerical scheme, which always happens after some amount of propagation time due to finite spatial and temporal grids, is signaled by a rapid increase of the energy. The simulation breaks down earlier for larger values of interaction  $g$ , because the length scale  $\xi \sim g^{-1/4}$  is smaller. With spatial grids of up to  $\sim 100$  per trap oscillator length, we obtained useful results up to  $g \lesssim 200$ .

Locating the vortex and antivortex is tricky, especially for smaller  $g$ . It is then often not sufficient to analyze the densities. One possibility is to observe both real and imaginary parts of  $\psi$  and find points where they both vanish; another tactic is to track phases and identify plaquettes around which there is a  $2\pi$  phase winding.

Our main observation is that the motion of the vortex dipole is never periodic, as opposed to the variational description. For small  $g$ , the motion is far more complicated. For larger  $g$ , the vortex pair starts to make almost closed orbits. Fig. 6 shows one of these relatively easier cases, at  $g = 150$ , where we have followed the dynamics for slightly longer than one ‘period’. As in the variational calculation, the competition between mutually

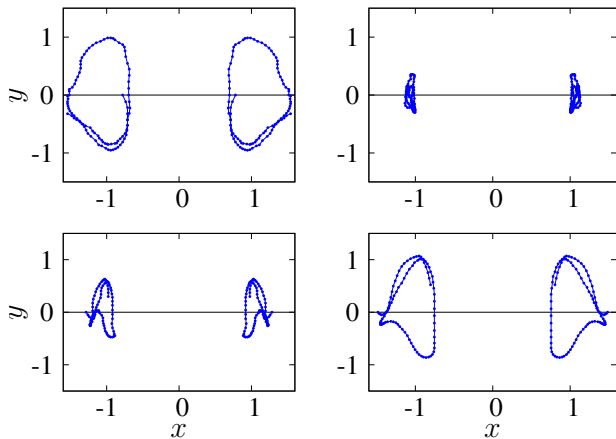


FIG. 7: (Color online.) Vortex pair trajectories from numerical solution of time-dependent GPE,  $g = 150$ . Starting positions are  $x_{1,2}(0) = 0.8, 1.1, 1.3,$  and  $1.5$ . Successive vortex/antivortex positions have been joined by straight lines. The condensate radius (Thomas-Fermi) is  $R_{\text{TF}} \simeq 3.72$ , not visible in these plots. Lengths are plotted in trap units.

driven and inhomogeneity-driven motion is clear, as is the tendency to reverse direction when the vortex dipole reaches the ‘edge’ of the condensate. There are several additional unexplained features. One is the structure at the outer edges of the orbits. Also, for large initial pair distances  $x_1(0) > x_s$ , we note that the defects first move in the  $-y$  direction for a very short time, before starting in the  $+y$  direction. These two features might be due to effects of the relatively nearby boundary [25, 28].

The situation is significantly more complicated for smaller  $g$ , as shown in Fig. 8. The vortex positions are joined by straight lines. The big jumps in these ‘trajectories’ represent intervals where the singularities were difficult to track or distinguish, or there were additional singularity pairs. The vortex and antivortex in the  $g = 50$  case each make almost one complete revolution around the stationary point, before coming too close to each other, and after this the situation for some time becomes too complicated to track. This is when the pair undergoes some type of ‘annihilation’, leading to some complicated excitations including additional singularity pairs. When we next manage to track a pair, they move again roughly along trajectories around the stationary point, until they come near each other again.

The  $g = 10$  case is even more complicated. For  $g < 18$ , there is no true stationary vortex dipole solution; therefore the paradigm of each defect rotating around a stationary position is not expected to provide a useful description. Nevertheless, some remnant of the pair ‘revolving around stationary positions’ seems to be visible in the defect trajectories.

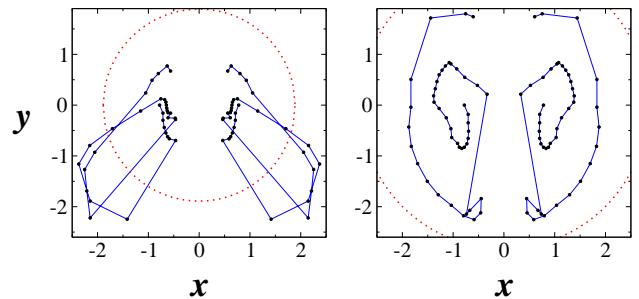


FIG. 8: (Color online.) Vortex pair trajectories from numerical evolution of time-dependent GPE,  $g = 10$  and  $g = 50$ . Starting positions are  $x_{1,2}(0) = \pm 0.8$ . Successive positions have been joined by straight lines. There are some gaps in time (widely separated points joined by a straight line). These correspond to intervals where the presence of several vortex-antivortex pairs made it difficult to meaningfully track a single pair. The Thomas-Fermi value for the condensate radius are  $R_{\text{TF}} \simeq 1.89$  and  $R_{\text{TF}} \simeq 2.825$  in the two cases, shown with dotted lines. Lengths are plotted in trap units.

## VI. DENSITIES

It is only at rather large  $g$ , when the vortex size  $\xi$  is small, that density plots are useful for identifying vortices. The middle figure in Fig. 6 shows that for  $g$  moderately above  $g_c \approx 18$ , the density profiles for stationary vortex dipole configurations look substantially like the stationary soliton case (Fig. 6 left). Obviously in a dynamic situation at such interactions, the vortices retain little of their individual identity as they move around, which helps explain why the singularity trajectories in Fig. 8 are not easy to explain in the vortex-antivortex language.

For  $g \sim 50-100$ , the vortices are more well-defined in stationary density profiles (Fig. 6 right), but still have significant shape dynamics when they are moving. It is only at very large  $g$  that the vortex and antivortex can be regarded as point objects. This is the case where the Lagrangian analysis, based on wavefunctions with well-defined vortices, gives good insight.

Density plots of the non-interacting Bose condensate with a ‘vortex dipole’ (Sec. III) typically show a ‘soliton’-like profile rather than distinct vortex and antivortex, indicating that the vortex picture is of limited relevance.

Our variational wavefunctions (A.2) and (A.3) also have large vortex sizes. As a result, when the pair distance is not very large, the density profile tends to show a large stripe of low-density region (*i.e.*, soliton-like profile) instead of individual depressions for vortex and antivortex. However, the distinct identities of the vortex and antivortex (as well as lack of additional dynamics possibilities) is built into these wavefunctions.

## VII. DISCUSSION

To summarize, we have analyzed, using several methods and viewpoints, the trajectories of a vortex-antivortex pair in a circularly trapped Bose-Einstein condensate, described by the Gross-Pitaevskii equation. The principal intuition we have provided is in terms of the competition between mutually-driven and inhomogeneity-driven motions of the pair. This leads to a simple understanding of the stationary vortex dipole solutions [13, 14], and also leads to the expectation of a type of motion where the vortex and antivortex each revolve around the stationary positions. Although our time-evolution simulations do not extend to interactions beyond  $g = 200$ , our available results strongly indicate that this type of pair motion becomes more and more relevant for larger interactions.

The fact that low- $g$  condensates show more complicated vortex dynamics has been given proper context through our considerations of the non-interacting case, the stationary solutions below and above  $g = g_c \approx 18$ , and density profiles, in Secs. III, IV, VI. At large  $g$ , the vortex shape distortion dynamics is less important (because they are smaller objects), there is lesser tendency of pairs to morph into or mimic soliton-like objects, extra pairs are not created as easily, and annihilation is less likely in the absence of dissipation. All this favors the type of motion described above, obtained from our variational wavefunction which only allows position dynamics for a single vortex dipole. At smaller  $g$ , the description in terms of vortex positions alone is less adequate, because of additional dynamics possibilities.

Vortex dipoles can be regarded as the two-dimensional analogs of dark solitons in one dimension, and of vortex rings in three dimensions. Each of these are solitary waves in uniform (untrapped) Bose condensates of the appropriate dimension, and can become non-propagating stationary objects in trapped condensates. Vortex rings in trapped 3D BECs display self-propelled and inhomogeneity-driven motions in opposite directions, just as we have found for vortex dipoles in 2D.

Our study opens up a number of additional questions.

1. As described in Sec. V, there are aspects of the trajectories that we do not understand even for relatively large  $g$ , such as the initial negative- $y$  motion for  $x_1(0) > x_s$  (Fig. 7). Presumably, this requires understanding of the coupling of the vortex position dynamics to the vortex shape dynamics. It is intriguing to ask whether the trajectory becomes smoother and more periodic at even larger  $g$ .
2. For small  $g$ , an additional open question is how the vortex dipole motion is affected by the presence of ‘nearby’ solitonic solutions, *e.g.*, this might explain the appearance of extra pairs. (A soliton may be regarded as a very large number of vortex dipoles.)
3. The ‘reflection’ of the dipole when it reaches the ‘edge’ of the condensate could be better studied in the setting of an elongated 2D condensate, where edges are better

defined than in our circular case.

4. There remains the open question of vortex dipoles which are initially not placed symmetrically around the trap center.

5. We have not studied the effects of dissipation on vortex dipole dynamics. In particular, dynamics of vortex pair creation and annihilation is important for Kosterlitz-Thouless physics [2]. At present we do not have a satisfactory theoretical framework for including such effects.

We hope to address some of these issues in future work.

## APPENDIX: VARIATIONAL FORMALISM

We describe here the variational Lagrangian formulation used in Sec. II to follow the motion of vortex and antivortex positions. Our results are based on variational wavefunctions of the form (2), where vortex positions appear as time-dependent variational parameters  $z_1(t)$  and  $z_2(t)$ . Using such a wavefunction in the Lagrangian

$$L = \int dr \left[ \frac{i}{2} \left( \psi^* \frac{\partial \psi}{\partial t} - \psi \frac{\partial \psi^*}{\partial t} \right) + \frac{1}{2} \psi^* \nabla^2 \psi - V_{\text{tr}}(\mathbf{r}) |\psi|^2 - \frac{1}{2} g |\psi|^4 \right], \quad (\text{A.1})$$

one can derive Euler-Lagrange equations of motion for the complex parameters  $z_1(t)$  and  $z_2(t)$ . Solving the equations of motion then provides the trajectories of the topological defects. This method for vortex dynamics in BECs was pioneered in Ref. [6] and has since been used in several vortex applications [21, 22, 23, 24, 25, 26].

For the condensate shape function  $f_c$  of Eq. (2), we used both Gaussian and Thomas-Fermi forms:

$$\psi_G = A_G(t) [z - z_1(t)] [z^* - z_2^*(t)] \exp[-|z|^2/2] \quad (\text{A.2})$$

and

$$\psi_{\text{TF}} = A_{\text{TF}}(t) [z - z_1(t)] [z^* - z_2^*(t)] f_{\text{TF}}, \quad (\text{A.3})$$

with  $f_{\text{TF}} = \sqrt{(\mu - \frac{1}{2}|z|^2)/g}$  and  $\mu = \sqrt{g/\pi}$ .

Here  $A(t)$  is a time-dependent normalization constant. Retaining this factor  $A(t)$  is essential for getting the dynamics even qualitatively correct. For example, for the single-vortex case, omitting this factor gives vortex precession in the *reverse* direction! Since  $A(t)$  actually contains the vortex position parameters  $z_{1,2}(t)$ , terms in the equations of motion are missed when  $A(t)$  is omitted.

Our form (2) is generalized from the lowest-Landau-level form for vortices in a rapidly rotating condensate [27]. It has the advantage of being amenable to exact treatment, *i.e.*, the integrations in (A.1) can be performed analytically. The disadvantage is that the vortices are ‘too big’, as discussed in Sec. II. We could in principle use any wavefunction of the form

$$\psi = A(t) g_v(u_1) e^{i\phi_1} g_v(u_2) e^{-i\phi_2} f_c(|z|^2) \quad (\text{A.4})$$

where  $u_i = |z - z_i|/\xi$  and  $\phi_i = \tan^{-1}(\frac{y-y_i}{x-x_i})$ . The vortex shape function  $g_v(u)$  ideally would be linear in  $u$  for  $u \rightarrow 0$  and constant for large  $u$  [3]; for example

$$g_v(u) = \frac{u}{\sqrt{u^2 + \xi^2}} \quad \text{or} \quad g_v(u) = 1 - e^{-u/\xi}.$$

Eq. (2) corresponds to  $g_v(u) = u$ , having the wrong behavior at large  $u$ . This is why our variational wavefunctions have unnaturally large vortices. Unfortunately, we were unable to identify a function  $g_v(u)$ , having the correct limiting behaviors, for which the integrals in Eq. (A.1) can be done analytically. We also did not attempt to incorporate velocity field effects due to the boundary [25, 28]. Our presented results are therefore limited to wavefunctions of the form of Eq. (2).

Using one of our variational wavefunctions, (A.2) or (A.3), the Euler-Lagrange equations of motion,  $D_t(\partial L/\partial \dot{u}) = \partial L/\partial u$ , become equations of motion for

the defect positions  $x_{1,2}(t)$  and  $y_{1,2}(t)$ . We can obtain these equations of motion analytically, but they are too cumbersome to reproduce here.

For a single vortex-antivortex pair with unrestricted positions, there are four variables, leading to four coupled first-order nonlinear differential equations which can be solved numerically for the vortex trajectory. For the initial conditions we have used, we expect the motion to be symmetric around the  $y$ -axis, so that we can use  $x_1(t) = -x_2(t)$  and  $y_1(t) = y_2(t)$ . This significantly reduces the numerical cost of solving the equations of motion, of which there are now only two.

## ACKNOWLEDGMENTS

MH thanks Henk Stoof for discussions and insights.

- 
- [1] D. R. Scherer, C. N. Weiler, T. W. Neely, and B. P. Anderson, *Phys. Rev. Lett.* **98**, 110402 (2007)
- [2] S. Stock, Z. Hadzibabic, B. Battelier, M. Cheneau, and J. Dalibard, *Phys. Rev. Lett.* **95**, 190403 (2005).  
Z. Hadzibabic, P. Krüger, M. Cheneau, B. Battelier and J. Dalibard, *Nature* **441**, 1118 (2006).
- [3] A. L. Fetter, *Phys. Rev. A* **138**, 429 (1965).
- [4] C. A. Jones and P. H. Roberts, *J. Phys. A: Math. Gen.* **15**, 2599 (1982).
- [5] D. S. Rokhsar, *Phys. Rev. Lett.* **79**, 2164 (1997).
- [6] A. A. Svidzinsky and A. L. Fetter, *Phys. Rev. Lett.*, **84**, 5919 (2000).
- [7] S. Komineas and N. Papanicolaou, *Laser Physics* **14**, 571 (2004).
- [8] S. Komineas and J. Brand, *Phys. Rev. Lett.* **95**, 110401 (2005).
- [9] M. R. Matthews, B. P. Anderson, P. C. Haljan, D. S. Hall, C. E. Wieman, and E. A. Cornell, *Phys. Rev. Lett.* **83**, 2498 (1999).
- [10] B. Jackson, J. F. McCann, and C. S. Adams, *Phys. Rev. A* **61**, 013604 (1999).
- [11] J. Ruostekoski and Z. Dutton, *Phys. Rev. A* **72**, 063626 (2005).
- [12] S. Komineas, *Eur. Phys. J. Spec. Top.* **147**, 133 (2007).
- [13] L.-C. Crasovan, V. Vekslerchik, V. M. Pérez-García, J. P. Torres, D. Mihalache, and L. Torner, *Phys. Rev. A* **68**, 063609 (2003).
- [14] M. Mottonen, S. M. M. Virtanen, T. Isoshima, and M. M. Salomaa, *Phys. Rev. A* **71**, 033626 (2005).
- [15] Q. Zhou and H. Zhai, *Phys. Rev. A* **70**, 043619 (2004).
- [16] V. Pietila, M. Mottonen, T. Isoshima, J. A. M. Huhtamaki, and S. M. M. Virtanen, *Phys. Rev. A* **74**, 023603 (2006).
- [17] A. Klein, D. Jaksch, Y. Zhang, and W. Bao, *Phys. Rev. A* **76**, 043602 (2007).
- [18] L. P. Pitaevskii, *Zh. Eksp. Teor. Fiz.* **40**, 646 (1961)[*Sov. Phys. JETP* **13**, 451 (1961)].
- [19] E. P. Gross, *Nuovo Cimento* **20**, 454 (1961).
- [20] C. Cohen-Tannoudji, B. Diu and F. Laloe, *Quantum Mechanics*, Vol. 1, Wiley, 1997. Chapter VI, Complement D.
- [21] E. Lundh and P. Ao, *Phys. Rev. A* **61**, 063612 (2000).
- [22] M. Linn and A. L. Fetter, *Phys. Rev. A* **61**, 063603 (2000).
- [23] A. L. Fetter, *Phys. Rev. A* **68**, 063617 (2003).  
J. Kim and A. L. Fetter, *Phys. Rev. A* **72**, 023619 (2005).
- [24] A. B. Bhattacharjee, O. Morsch and E. Arimondo, *J. Phys. B: At. Mol. Opt. Phys.* **37** 2355 (2004).
- [25] U. Al Khawaja, *Phys. Rev. A* **71**, 063611 (2005).
- [26] M. Snoek and H. T. C. Stoof, *Phys. Rev. Lett.* **96**, 230402 (2006); *Phys. Rev. A* **74**, 033615 (2006).
- [27] Tin-Lun Ho, *Phys. Rev. Lett.*, **87**, 060403 (2001).
- [28] J. R. Anglin, *Phys. Rev. A* **65**, 063611 (2002).